Available online at www.sciencedirect.com
SCIENCE DIRECT
Cement and Concrete Research 36 (2006) 1345–1353
Cement and Concrete Research

Fracture of model concrete: 2. Fracture energy and characteristic length

C. Rosselló, M. Elices *, G.V. Guinea

Departamento de Ciencia de Materiales, Universidad Politécnica de Madrid E.T.S.I. Caminos, Profesor Aranguren s/n. 28040-Madrid. Spain

Received 12 April 2005; accepted 16 April 2005

Abstract

The specific fracture energy G_F was measured in six types of simple concrete: all from the same matrix. The aggregates were spheres of the same diameter (strong aggregates, that debonded during concrete fracture, and weak aggregates, able to break); three kinds of matrix–aggregate interface (weak, intermediate and strong) were used. All in all, 55 test results are reported. These results are intended to be used as an experimental benchmark for checking numerical models of concrete fracture.

A meso-level analysis of these results showed a correlation between the measured G_F values and the properties of the matrix, aggregates and interfaces, particularly with the actual area of the fracture surface. The strength of the matrix–aggregate interface correlates quite well with G_F, and concrete ductility, measured by means of the characteristic length, correlates also with the strength of the matrix–aggregate interface.

Keywords: Concrete; Fracture; Fracture energy; Toughness; Debonding

1. Introduction

This paper is a sequel to a previous one by the same authors [1]. The purpose of both papers is to offer experimental results that can be profitably used for concrete research and design, and they are intended to serve as an experimental benchmark for checking numerical models of the mechanical behaviour of concrete.

This second paper provides experimental values of the specific fracture energy G_F for very simple concretes: all made with the same matrix, with two types of spherical aggregates and three kinds of matrix–aggregate interfaces. It is hoped that these results may provide hints for the design of concretes with higher G_F values [see, for example Ref. [2]]. There is an increasing awareness that in some cases tensile strength and modulus of elasticity are not enough to characterize the mechanical response of concrete, particularly when ductility or toughness are of concern [see, for example, Refs. [3–7]], and suggestions in this direction should also be welcome.

The paper addresses the fracture energy of concrete as defined within the context of the cohesive crack model. However, the results are far reaching as this property can be defined not only within the framework of cohesive models and it has become a reference parameter in the field of concrete fracture.

The paper is structured in the following way: First, a report of the experimental results of the measurements of G_F for the different concretes; then a mesoscopic analysis of these results based on the roughness of the fracture surfaces, the type of aggregates, and the role of the matrix–aggregate interface, and finally, some recommendations to improve G_F and concrete toughness.

2. Measurement of the fracture energy

This section provides experimental results of the specific fracture energy, G_F, of a simple concrete in the hope that these values could be used for checking numerical models of concrete failure. All the concretes were made with the same matrix, two kinds of aggregates and three matrix–aggregate interfaces, as detailed in a previous paper [1].

2.1. Theoretical background

The ideal direct procedure to measure G_F is by means of a stable uniaxial tensile test. Unfortunately, it is difficult to perform stable and representative tensile tests [8], and a simpler

* Corresponding author.
E-mail address: melices@mater.upm.es (M. Elices).

0008-8846/$ - see front matter © 2006 Elsevier Ltd. All rights reserved.
doi:10.1016/j.cemconres.2005.04.016

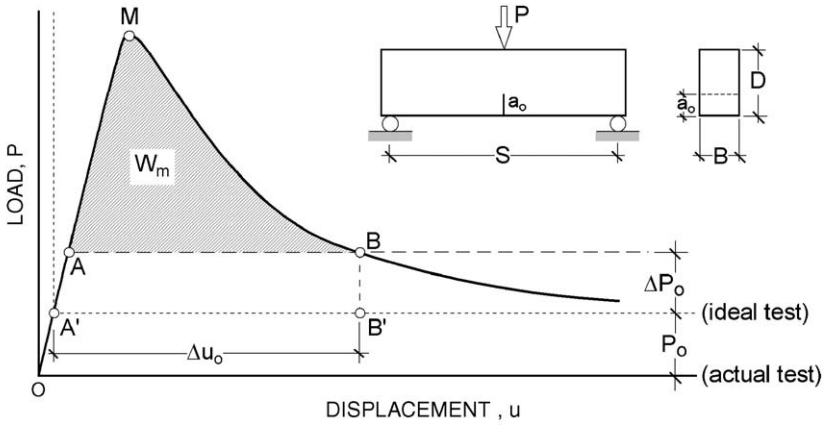

Fig. 1. Load-displacement curve for an overcompensated test where the dead forces —not shown in the figure— produce a negative bending moment and the residual load is P_0, exaggerated for clarity. (Notice the different axes for the actual test and the ideal one).

procedure, based on the measure of the total work of fracture of three-point bend notched beams, proposed by RILEM TC-50 [9], was used in this research.

If W_F is the work supplied to statically fracture the notched specimen, G_F can be computed as:

$$G_F = \frac{W_F}{B(D-a_0)} \tag{1}$$

where B is the beam thickness and $D-a_0$ is the ligament length (as shown in Fig. 1).

A detailed analysis of this test can be found in the book of Bazant and Planas [10] and the possible sources of error in the measurement of the work supply were analyzed by Guinea, Planas and Elices [11–13]. Using the perturbed ligament model, the authors managed to represent adequately their observed results [23–26]. Hu and Wittman also dealt with this problem and addressed the possibility that the fracture energy may not be constant along the crack path [27–29]. At present, the simplest hypothesis of assuming G_F to be constant is sufficient for the purpose of this article. It suffices to point out that the weight of the specimen contributes to the overall loading of the system and has to be considered. Here, we use the *weight compensation* procedure, as described in Ref. [10], to account for the specimen weight.

In practice, *exact* weight compensation cannot be achieved, and one has to work with a slight overcompensation, so that the dead forces produce a negative bending moment and the residual load at the end of the tail of the test is equal to P_0, as shown in Fig. 1. This figure shows a load-displacement curve for an overcompensated test, as occurs in practice. Usually the test is stopped at B, before the specimen is fully broken. Dotted axes should correspond to an ideal test in which the specimen is broken into two halves, and the P_0 value is exaggerated for clarity.

The measured work W_m (the area $AMBA$, in Fig. 1) is, in general, a value very near the actual work needed to fracture the notched beam W_F. The correction for the missing area $A'AB \infty B'A'$ (greatly exaggerated, for clarity, in the figure) can be computed as shown in Refs. [10,14]. The total work supplied to fracture the beam is:

$$W_F = W_m + 2\cdot\Delta u_0 \Delta P_0 = W_m + 2\cdot\frac{BS}{4\Delta u_0}\zeta \tag{2}$$

where (see Fig. 1) ΔP_0 is depicted in the figure, $\Delta u_0 = A'B'$ is almost equal to AB, the beam thickness is B, the length between supports is S, and ζ is the first order moment of the softening function (a material parameter, under the assumption of a cohesive crack model). Alternatively, when the softening function is unknown, the expression $BS\zeta/4 \equiv \Lambda$ can be obtained by least square fitting of

$$P - P_B = \Lambda\left[\frac{1}{(u-u_A)^2} - \frac{1}{(u_B-u_A)^2}\right] \tag{3}$$

as explained in Ref. [13]. (Notice that u_A is almost equal to $u_{A'}$, being much less than u_B).

There has been some misunderstanding regarding the factor 2 in Eq. (2), as in [15,16]. It was due to a confusion between areas

Table 1
Average composition of the model concrete

Component	Cement	Sand	Aggregate	Water	Silica fume	Plasticizer (Sikamet 300®)
kg/m^3	482	938	544	157	42	32
dm^3/m^3	153	354	258	157	22	26

Table 2
Mechanics properties of matrix and aggregates

	Modulus of elasticity (GPa)	Tensile strength (MPa)	Fracture energy (J/m2)
Matrix	31±2	4.7±2	52±6
Strong aggregate	19±2	16±2	>60 *
Weak aggregate	2.1±0.5	1.7±0.3	<40 *

* Ref [21].

Table 3
Fracture energy, G_F, and percentage of debonded aggregates, PA, in the broken section, for concrete with strong spheres and different kinds of matrix–aggregate interfaces

Medium interface (No surface treatment)	G_F (J/m^2)	55.7	57.1	60.7	62.1	65.1	66.6	68.3	70.1	77.2	79.1	**66.2**
	PA (%)	9.4	11.5	7.6	13.3	16.1	16.3	11.1	20.0	8.2	13.1	**12.7**
Medium interface (Surface treatment with a release agent)	G_F (J/m^2)	51.0	52.3	53.7	54.5	54.8	55.7	64.9	66.5	69.7	74.6	**59.8**
	PA (%)	13.1	6.4	15.2	8.1	18.2	13.1	12.9	23.9	4.8	13.8	**13.0**
Weak interface (almost no bonding between matrix–aggregate)	G_F (J/m^2)	37.5	39.9	44.8	49.7	49.9	51.1	51.3	54.8	57.9	*	**48.5**
	PA (%)	34.7	29.6	21.1	34.1	32.1	19.5	31.2	31.0	23.0	*	**28.5**

(*) No data available. Failed test.
Bold figures indicate average values.

(*AMBA*) and (*A′MBB′A′*) —the last one cannot be experimentally measured—. The justification of this factor 2 can be seen in Refs. [10,14]. Sometimes, confusion has arisen because the cohesive crack was not accepted as a suitable model for concrete failure. A recent paper on the choice of a fracture test for concrete and its statistical evaluation, by Bazant et al. [17], reviews the advantages of this method.

2.2. Experimental results

We designed simple concrete, able to be modeled without too much effort: The *matrix* was a mortar of cement and sand, the same as for all types of concrete. The *aggregates* were of commercial spheres of mullite, of an average diameter of 7.4 mm. Two kinds of sphere were considered; the strong ones —with an average tensile strength of 16 MPa— intended not to be broken during the fracture test, and the weak ones —with an average tensile strength of 1.7 MPa—, so that some would break when testing the beams. Three kinds of *matrix–aggregate interface* were devised; weak, strong and intermediate interfaces. The estimated debonding energies of the matrix–aggregate interfaces were, according to Ref. [1]: weak interfaces 10 ± 10 J/m^2, intermediate interfaces 30 ± 10 J/m^2, and strong interfaces 50 ± 10 J/m^2. The concrete mix is shown in Table 1. The water/cement ratio, by weight, was 0.32. The percentage, in volume, of aggregates was 25.8. The mechanical properties of matrix and aggregates are summarized in Table 2. All in all, six types of concrete were designed and tested. The detailed properties of the components and those of sample manufacture were given in a previous paper [1].

The notched beams were tested according to the RILEM recommendations [9]: 30 beams were made with strong aggregates (beam depth 40 mm) and another set of 30 beams was made with weak aggregates (beam depth 40 mm). Load-CMOD (Crack Mouth Opening Displacement) and load-displacement curves were recorded and the results were published in Ref. [1].

From the load-displacement records, the work of fracture W_F was computed by applying Eq. (2), where the term $BS\zeta/4$ was obtained by the least square fitting of Eq. (3), according to Refs. [10,13]. Finally, the specific fracture energy G_F was computed using Eq. (1).

2.2.1. Beams with strong aggregates

Table 3 gives the values of G_F for the three sets of concrete beams made with strong spheres. As expected, no broken aggregates were found on the fracture surface; only debonded spheres were recorded. The percentage of debonded aggregates (PA) relative to the broken section, defined as

$$\mathrm{PA} = \frac{\text{projected surface of debonded aggregates}}{\text{projected broken surface}} \times 100$$

was also measured and appears in Table 3.

Fig. 2 shows the measured specific fracture energy G_F as a function of the percentage of debonded aggregates in the broken section, PA. Although three different surface treatments were

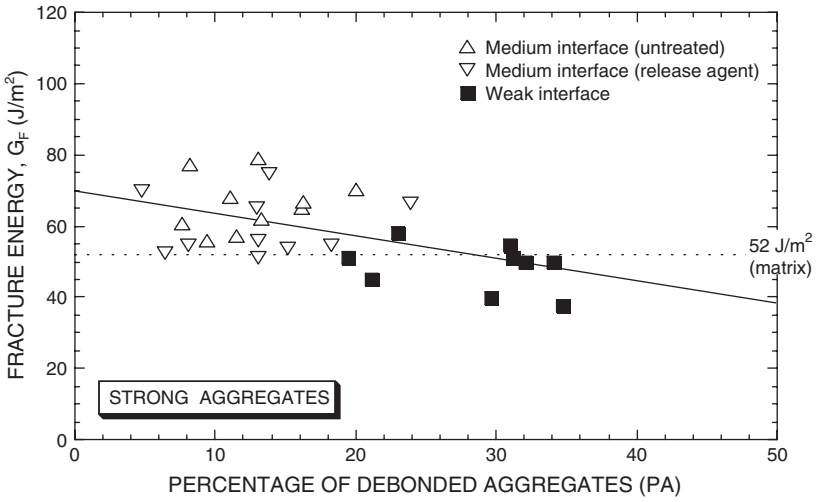

Fig. 2. Fracture energy G_F as a function of the debonded aggregates, for concretes made with strong spheres and different kinds of matrix–aggregate interfaces. The horizontal dashed line marks the average fracture energy of the matrix (52 J/m^2).

initially devised, only two types of matrix–aggregate interfaces were finally achieved: an intermediate one, with aggregates without treatment and also with aggregates daubed with a commercial release agent (Sika E); and a weak one, when a polymer coating of the aggregates created a very weak aggregate–matrix bond (as explained in Ref. [1]).

Looking at Fig. 2 and at the fracture surfaces, one realizes that the presence of bonded strong aggregates forces the crack path to wander around them, increasing the actual fracture area, and increasing the work of fracture W_F and, consequently of G_F. Notice that the fracture energy of the matrix is 52±6 J/m^2 [1]. As the percentage of debonded aggregates in the broken section increases, the fracture energy decreases. This is particularly evident for beams made with unbonded (or almost unbonded) spheres. Very briefly, it appears that as the matrix–aggregate interfaces become weak, the fracture energy decreases, and the crack path changes from predominantly through the matrix to one through the matrix–aggregate interfaces, a fact reflected by the values of PA.

2.2.2. Beams with weak aggregates

Table 4 gives the values of G_F for the three sets of concrete beams made with weak spheres. Each set corresponds to a kind of matrix–aggregate interface; weak interfaces were achieved with aggregates treated with a release agent (Sika E), untreated aggregates provided intermediate strength interfaces, and strong interfaces were obtained with an epoxi polymer (in this case, due to a higher porosity and roughness of the weak aggregate surface, we succeed in bonding the matrix and aggregates).

As planned, some aggregates were found broken on the fracture surface. The percentage of broken aggregates relative to the total aggregate surface on the broken section (PBA) was defined as:

$$\mathrm{PBA} = \frac{\text{projected surface of broken aggregates}}{\text{projected surface of aggregates}} \times 100 \qquad (5)$$

Values of PBA are reported in Table 4.

Fig. 3 shows the measured fracture energy G_F as a function of the percentage of broken aggregates, PBA. When the matrix–aggregate interface is weak, most of the aggregates are debonded —the PBA ranges between 0% and 15%— and the fracture mechanism is the same as that in beams made with strong aggregates. The measured values of G_F for weakly bonded aggregates vary between 30 and 50 J/m^2, and compare well with the interval of 40–80 J/m^2 shown in Fig. 2 for strong aggregates weakly bonded. As the matrix–aggregate interface becomes stronger, and more aggregates break, the fracture energy G_F increases and reaches maximum values when the interface is very strong and all the particles in the section appear broken. Notice that the maximum values recorded (63 and 64.4 J/m^2) are lower than the maximum values measured with debonded strong aggregates (79.1 J/m^2).

3. Mesoscopic approach

The values of the specific fracture energy G_F were obtained by dividing W_F, the measured work of fracture, by $B(D-a_0)$, the projected area of fracture according to the RILEM recommendation [9]. Inspection of the fractured surfaces showed different degrees of roughness —depending on the type of aggregate and matrix–aggregate interfaces— and hence different values of the actual areas, although all surfaces had the same projected area. A knowledge of the fracture energy expended per unit of actual area, instead of the projected area, may cast some light on the fracture processes at the meso-level —where the aggregates, matrix and interfaces are considered— and is the subject of this section.

3.1. Measurement of the actual fracture surfaces and fracture energy

The topographic analysis of the crack surfaces from the notched beam tests was performed with a laser profilemeter, as described in Ref. [7]. The profiles were measured parallel to the initial crack front and spaced 2 mm (15 profiles in the broken section of each beam, where $D-a_0=30$ mm). The profile points were recorded every 0.2 mm, with the same resolution, 0.2 mm, in height. The surface was measured on one of the cracked

Table 4
Fracture energy, G_F, and percentage of broken aggregates, PBA, for concretes with weak spheres and different kinds of matrix–aggregate interfaces

Strong interface (epoxi coated aggregates)	G_F (J/m^2)	50.5	56.7	58.3	61.0	61.2	63.0	64.4	*	*	*	**59.3**
	PBA (%)	100	100	100	100	89	100	100	*	*	*	**98.4**
Medium interface (no surface treatment)	G_F (J/m^2)	32.2	34.4	36.2	36.6	37.4	38.6	40.8	44.2	48.3	49.8	**39.8**
	PBA (%)	26	45	43	54	24	49	52	29	25	63	**41.0**
Weak interface (surface treatment with a release agent)	G_F (J/m^2)	28.9	36.5	37.3	38.0	42.2	42.3	43.2	47.3	50.2	n.d	**40.6**
	PBA (%)	0	0	10	10	0	15	0	13	11	n.d	**6.5**

(*) No data available. Failed test.
Bold figures indicate average values.

halves of the specimens. All in all, 55 fracture surfaces were measured.

From the actual fracture surface area, the actual specific fracture energy G_F^* can be determined as:

$$G_F^* = \frac{W_F}{\text{Actual fractured surface}}, \tag{6}$$

3.2. The fracture energy G_F, revisited

3.2.1. Beams with strong aggregates

Fig. 4 shows the *actual* specific fracture energy G_F^*, as a function of the percentage of aggregates debonded in the broken section, PA. A least squares straight line fit of these results (G_F^*=53–0.62 PA) is shown in the figure. The expected scatter band (the same as for the matrix values) is also drawn.

Some aspects of this figure are worth a comment. Since the crack path is always through the matrix or follows the weaker matrix–aggregate interface —no broken aggregates were found— the *actual* fracture energy G_F^* will always be equal to or lower than the average matrix fracture energy G_F (52 J/m^2). (We found that G_F (matrix) ≈ G_F^* (matrix), because the fracture surfaces of mortar samples were quite smooth, as compared to concrete ones). Most of the G_F^* values lie inside the scatter band shown in Fig. 4. The vertical intercept of the regression line (53 J/m^2) is close to the average value of the matrix, as it should be because in this limit is PA=0% and all fracture is confined in the matrix surrounding the aggregates.

The results in Fig. 4 fit well with a simple estimate for G_F^*, obtained by adding the contributions of the matrix and the matrix–aggregate interface:

$$G_F^* = G_F^*(\text{matrix}) \times (1-\text{PA}/100) + G_F^*(\text{interface}) \times (\text{PA}/100), \tag{7}$$

Extrapolation of the linear fit in Fig. 4 to PA=50% (22 J/m^2) gives a fracture energy close to half the matrix fracture energy, as it should be if the value of G_F^* (interface) in Eq. (7) was 0, the corresponding value for unbonded aggregates.

3.2.2. Beams with weak aggregates

Fig. 5 shows the *actual* specific fracture energy G_F^* as a function of broken aggregates (PBA) for concrete beams made with weak aggregates and three kinds of matrix–aggregate interfaces: weak, intermediate and strong.

It is apparent, from these results, that all G_F^* values are below the matrix fracture energy, except two values for strong bonded aggregates that are similar, taking into account the scatter band. Another interesting result that confirms previous ones is that G_F^* decreases as the matrix–aggregate interface strength decreases.

A detailed analysis of concretes made with soft aggregates weakly bonded, shows values of G_F^* between 20 and 30 J/m^2, in accordance with the expected values for concretes made with strong and unbonded aggregates with PA values between 30%

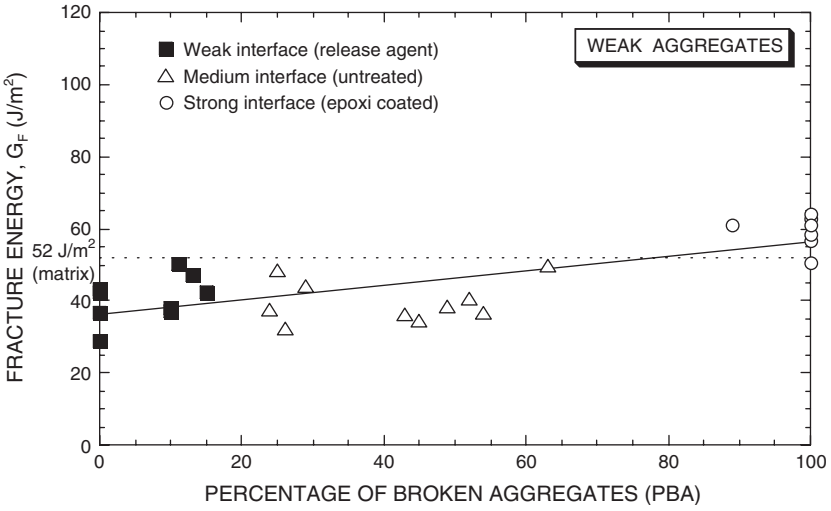

Fig. 3. Fracture energy G_F as a function of the broken aggregates, for concretes made with weak spheres and different kinds of matrix–aggregate interfaces. The horizontal dashed line marks the average fracture energy of the matrix (52 J/m^2).

and 36% (see Fig. 4). The measured PA values in the four tests with PBA = 0 are 31%, 35%, 36% and 36%.

When the weak aggregates are strongly bonded to the matrix, almost all aggregates on the fracture surface are broken; PBA = 100% in six of the seven valid tests and PBA = 89% in the remaining. Here, although extra work was required to break the aggregates, all the mean values of the actual fracture energy G_F^* remained below the matrix value. The scatter found in G_F^* values for PBA = 100% (from 31 to 50 J/m^2) deserves further research, as the recorded values of relative areas of broken aggregates and their expected fracture energy are not enough to account for these results.

4. Concrete brittleness

The fracture energy G_F alone does not suffice to characterize the ductility/brittleness of concrete and its dependence on the size of the structure. Instead, the brittleness number proposed by Hillerborg [22] captures both the influence of the material and that of the size of the structure by means of the ratio

$$\beta = \frac{l}{l_{ch}} \tag{8}$$

where l is any structural dimension and l_{ch} a material parameter known as the characteristic length, defined by the ratio

$$l_{ch} = \frac{EG_F}{f_t^2} \tag{9}$$

where E is the modulus of elasticity and f_t is the tensile strength. The higher the brittleness number of a given structure, the lower the ductility.

Note that l_{ch} is proportional to G_F (a high fracture energy leads to a tougher concrete) but it also has a marked inverse

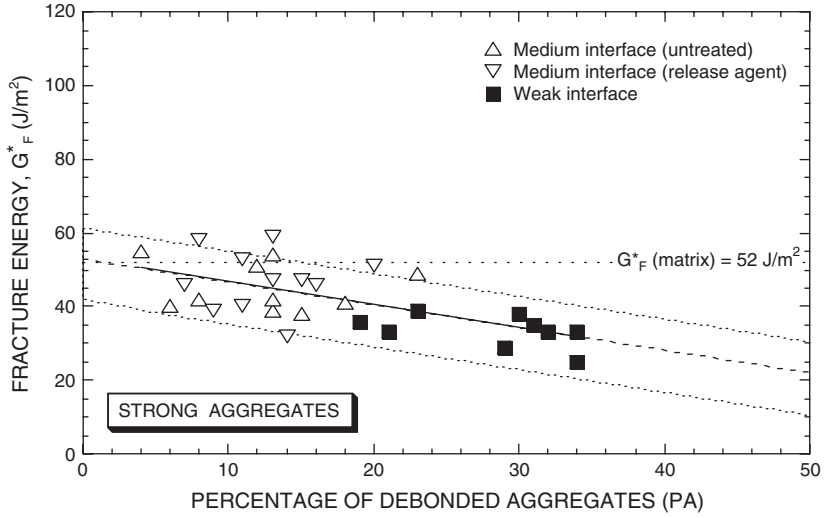

Fig. 4. Actual fracture energy G_F^* as a function of the debonded aggregates for concretes made with strong spheres and different kinds of matrix–aggregate interfaces and corresponding regression line.

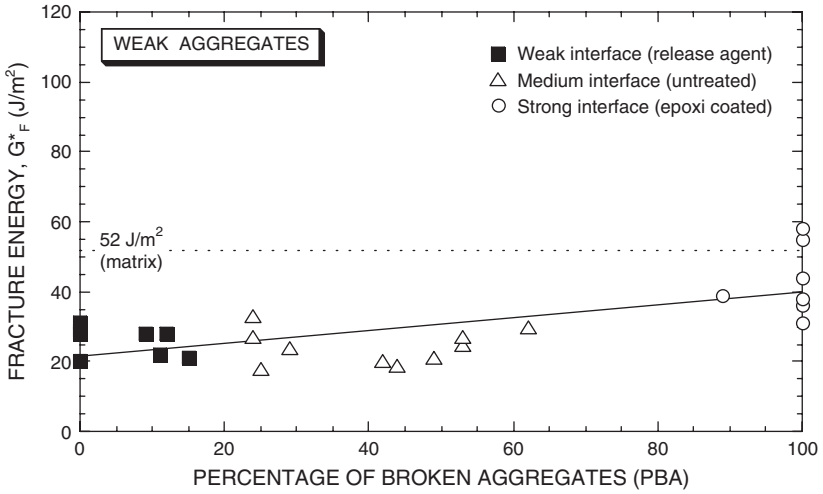

Fig. 5. Actual fracture energy G_F^* as a function of the broken aggregates for concretes made with weak spheres and three kinds of matrix–aggregate interfaces.

dependence on f_t (strong concretes are brittle), so a balance between the fracture energy and tensile strength is required to produce ductile concretes.

Over the years, there have been other proposals for brittleness numbers, most of them closely connected with Eq. (8). Because of its simplicity, the proposal by Hillerborg has become popular, and the characteristic length, l_{ch}, is now a standard measure of concrete toughness.

Fig. 6 shows the characteristic length for beams with strong aggregates as a function of the percentage of debonded aggregates, PA. Although the results show a great variability —due to the accumulated scatter of G_F and f_t in Eq. (9)— no definite trend is observed. The f_t values were taken from Ref. [1]. The characteristic length seems to be fairly insensitive to the performance of the interface, and holds constant over the matrix value when the interfacial strength is reduced in the range 0–35%PA.

The same tendency —with appreciably more scatter— is observed in beams with weak aggregates, Fig. 7. The transition from debonded to broken aggregates is not reflected in the l_{ch} values. The mean figures of l_{ch} are comparable in the two kinds of concrete: 92±8 mm for beams with strong aggregates and 106±12 mm for weak ones.

5. Final comments and conclusions

We mentioned at the beginning of this paper that there is an increasing awareness that tensile strength and elastic modulus are not enough to characterize the mechanical response of concrete when ductility or toughness are of concern, and that in these circumstances, concrete has to be designed with higher values of G_F and/or l_{ch}. This study gives some hints in this direction.

The highest G_F values were obtained with strong aggregates well bonded to the matrix (see in Fig. 2, the region where the percentage of debonded aggregates is low). The reason is that the crack path avoids the aggregates and wanders through the matrix, increasing the fracture area and hence the work of fracture W_F. When this work is divided by the actual area —and not the projected area— the matrix value is recovered as is

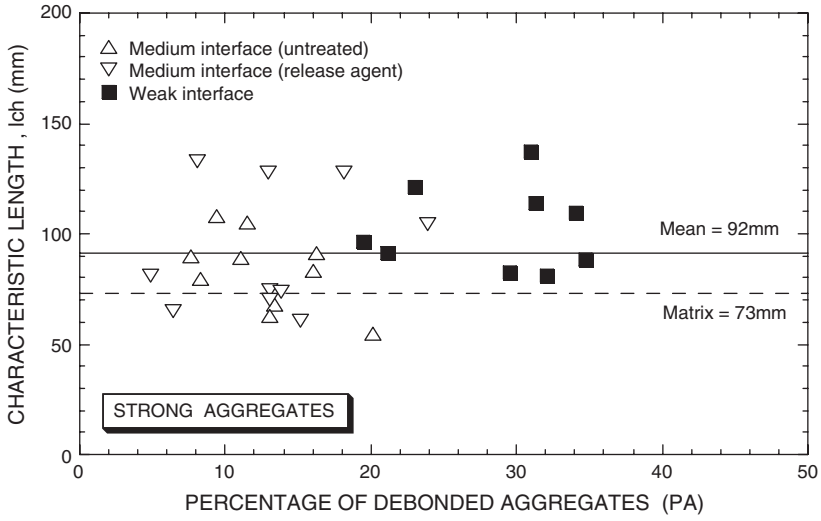

Fig. 6. Characteristic length l_{ch} as a function of the debonded aggregates for concretes made with strong spheres and different kinds of matrix–aggregate interfaces.

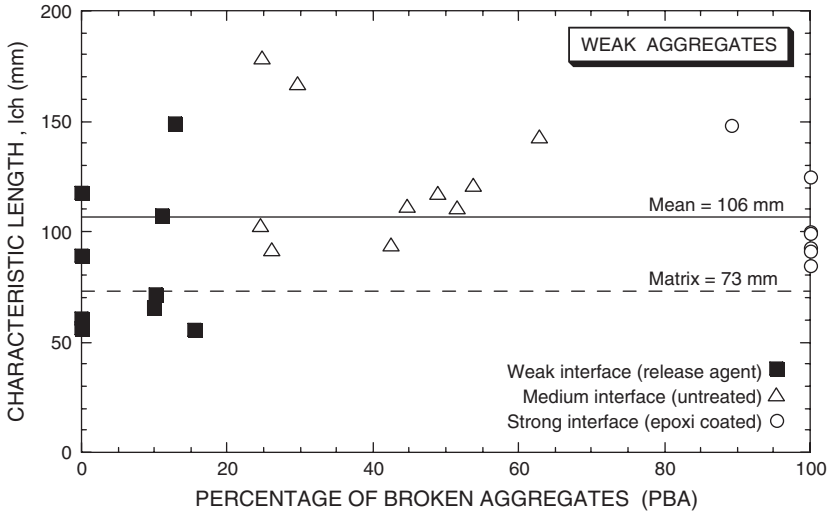

Fig. 7. Characteristic length l_{ch} as a function of the broken aggregates for concretes made with weak spheres and three kinds of matrix–aggregate interfaces.

shown in Fig. 4. Therefore, a strategy for increasing G_F is to increase the tortuosity of the crack path.

When weak aggregates are used, the highest G_F values are recorded when the matrix–aggregate interface is stronger and all the aggregates appear broken across the crack path. (See in Fig. 3, the values where the percentage of broken aggregates is 100%). Here —when the interface is strong— the crack path minimizes the work of fracture by crossing the aggregates instead of wandering through them. This is confirmed when W_F is divided by the actual area of the broken section, giving values of actual fracture energy below (or equal to) the matrix fracture energy. (Fig. 5).

As already mentioned, concrete brittleness is associated with the characteristic length l_{ch}, which increases with the presence of aggregates on the broken section but appears to be mostly insensitive to the interfacial strength (Figs. 6 and 7).

One conclusion that emerges from this research, done with a very simple concrete, is that —with a given aggregate— increasing the strength of the matrix–aggregate interface is the best way to increase G_F. As regards brittleness, the increase in G_F counterbalances the increase in tensile strength, f_t (see Eq. (9)) and the characteristic length remains almost constant.

The meso-level approach —that takes into consideration the roles of the matrix, aggregates, and the matrix–aggregate interface— should help in designing concretes with higher fracture energy or higher ductility. By measuring the actual surface fracture area, it has been possible to isolate this effect from the quality of the aggregates (strong or weak) and from the type of matrix–aggregate interface (see Figs. 4 and 5). This is particularly clear when the fracture surfaces exhibit only debonded aggregates, because the absence of broken aggregates makes the analysis easier. When the interface is very weak and it can be assumed that aggregates are initially debonded, it is quite easy to compute G_F from the values of the matrix fracture energy and the actual fracture surface through the matrix. Regarding ductility, the analysis is more involved due to the other variables concerned (E and f_t) and their dependence on the interfacial strength and the roughness of the crack path.

The second objective of this research was to provide experimental data of G_F that may serve as an experimental benchmark for checking numerical models of concrete fracture, in particular numerical concrete [18] or meso-level models [see, for example, Refs. [16,19,20]]. A summary of the mechanical properties of the matrix, aggregates and debonding energies of the matrix–aggregate interfaces are given in the paper, particularly in Table 2 and Ref. [1].

Acknowledgements

The authors gratefully acknowledge the useful discussions with Profs. Jaime Planas and Claudio G. Rocco. Support for this research was provided by the Spanish Ministry of Ciencia y Tecnología, under the grants MAT2000-1355 and FEDER UNPM 00-33-004.

References

[1] C. Rosselló, M. Elices, Fracture of model concrete: 1. Types of fracture and crack paths, Cem. Concr. Res. 34 (2004) 1441–1450.
[2] P.J.M. Monteiro, P.R.L. Helene, S.H. Kang, Design concrete mixtures for strength, elastic modulus and fracture energy, Mater. Struct. 26 (1993) 443–452.
[3] L. Elfgren, S.P. Shah (Eds.), Analysis of Concrete Structures by Fracture Mechanics, Chapman and Hall, 1991.
[4] C. Vipulanandan, W.H. Gerstle (Eds.), Fracture Mechanics for Concrete Materials Testing and Applications, ACI SP, vol. 201, 2001.
[5] B. Jakobsen, The status of LWA concrete and its use in offshore concrete floating platforms, FIP Notes (1994) 10–14.
[6] M. Elices, G.V. Guinea, J. Planas, Choosing the right concrete for piles, An application of concrete fracture mechanics, in: Z. Bazant (Ed.), Fracture Mechanics of Concrete Structures, 1993, pp. 782–787.
[7] G.V. Guinea, K. El-Sayed, C.G. Rocco, M. Elices, J. Planas, The effect of the bond between the matrix and the aggregates on the cracking mechanism and fracture parameters of concrete, Cem. Concr. Res. 32 (2002) 1961–1970.
[8] D.A. Hordijk, Deformation-controlled uniaxial tensile tests on concrete, Delft University of Technology Report 25.5.89-15 VFA, 1989.
[9] RILEM Draft, 50 FMC draft recommendation, determination of the fracture energy of mortar and concrete by means of three-point bend tests on notched beams, Mater. Struct. 18 (106) (1985) 285–290.

[10] Z.P. Bazant, J. Planas, Fracture and Size Effect in Concrete and other Quasibrittle Materials, CRC Press, 1998.
[11] G.V. Guinea, J. Planas, M. Elices, Measurement of the fracture energy using three-point bend tests: Part 1 — Influence of experimental procedures, Mater. Struct. 27 (1992) 99–105.
[12] J. Planas, M. Elices, G.V. Guinea, Measurement of the fracture energy using three-point bend tests: Part 2 — Influence of the bulk energy dissipation, Mater. Struct. 25 (1992) 305–312.
[13] M. Elices, G.V. Guinea, J. Planas, Measurement of the fracture energy using three-point bend tests: Part 3 — Influence of cutting the P-d tail, Mater. Struct. 25 (1992) 327–334.
[14] M. Elices, G.V. Guinea, J. Planas, On the measurement of concrete fracture energy using three-point bend tests, Mater. Struct. 30 (1997) 375–376.
[15] B. Cotterell, Y.W. Mai, Fracture Mechanics of Cementitious Materials, Blackie Academic and Professional, 1996.
[16] J.G.M. van Mier, Fracture Processes of Concrete, CRC Press, 1997.
[17] Z.P. Bazant, Q. Yu, G. Zi, Choice of standard fracture test for concrete and its statistical evaluation, Int. J. Fract. 118 (2002) 303–337.
[18] P.E. Roelfstra, H. Sadouki, F.H. Wittman, Le béton numérique, Mater. Struct. 18 (1985) 327–335.
[19] A. Carpinteri, M. Aliabadi (Eds.), Computational Fracture Mechanics in Cocrete Technology, WIT Press, 1999.
[20] G. Lilliu, J.G.M. van Mier, 3D lattice type fracture model for concrete, Eng. Fract. Mech. 70 (2003) 927–941.
[21] J.Y. Pastor, C.G. Rocco, A. Jones, private communication.
[22] A. Hillerborg, M. Modeer, P.E. Petersson, Analysis of crack formation and crack growth in concrete by means of fracture mechanics and finite elements, Cem. Concr. Res. 6 (1976) 773–782.
[23] P. Maturana, J. Planas, M. Elices, Evolution of fracture behaviour of saturated concrete in the low temperature range, Int. Conf. Fracture and Damage of Concrete and Rock. Vienna, 1988.
[24] J. Planas, M. Elices, Conceptual and experimental problems in the determination of the fracture energy of concrete, in: H. Mihashi, H. Takahashi, F.H. Wittman (Eds.), Fracture Toughness and Fracture Energy, Balkema, 1989, pp. 165–181.
[25] J. Planas, P. Maturana, G.V. Guinea, M. Elices, Fracture energy of water saturated and partially dry concrete at room temperature and at cryogenic temperatures, 7th. Int. Congress Fracture ICF7. Houston, 1989.
[26] P. Maturana, J. Planas, M. Elices, Evolution of fracture behaviour of saturated concrete in the low temperature range, Eng. Fract. Mech. 35 (1990) 827–834.
[27] X.Z. Hu, Fracture Process Zone and Strain Softening in Cementitious Materials, ETH Building Materials Reports No. 1. ETH Switzerland. AEDIFICATIO Pub., 1990.
[28] X.Z. Hu, F.H. Wittman, Fracture energy and fracture process zone, Mater. Struct. 25 (1992) 319–326.
[29] K. Duan, X.Z. Hu, F.H. Wittman, Boundary effect on concrete fracture induced by non-constant fracture energy distribution, in: R. de Borst, et al., (Eds.), Fracture Mechanics of Concrete Structures, 2001, pp. 49–55.